PHYSICAL REVIEW B **66**, 241308(R) (2002)

Acoustical and optical magnetoplasma excitations in a bilayer electron system

S. V. Tovstonog,[1,2] L. V. Kulik,[1,2] I. V. Kukushkin,[1,2] A. V. Chaplik,[3] J. H. Smet,[1], K. V. Klitzing,[1] D. Schuh,[4] and G. Abstreiter[4]

[1]*Max-Planck-Institut für Festkörperforschung, Heisenbergstrasse 1, 70569 Stuttgart, Germany*

[2]*Institute of Solid State Physics, RAS, Chernogolovka, 142432 Russia*

[3]*Institute of Semiconductor Physics, RAS, Siberian Branch, Novosibirsk, 630090 Russia*

[4]*Walter Schottky Institute, Technische Universität München, Am Coulombwall, D-85748 Garching, Germany*

(Received 13 June 2002; published 31 December 2002)

The charge-density magnetoexcitations in the bilayer electron system have been studied by means of inelastic light-scattering spectroscopy. Two principal magnetoplasma excitations of different symmetry, acoustical and optical magnetoplasmons, were observed. These principal excitations couple with in-phase and out-of-phase Bernstein modes at nonzero in-plane momentum through the many-body Coulomb interaction. Detailed measurements of the coupled mode energies were performed and compared with theoretical calculations.

DOI: 10.1103/PhysRevB.66.241308 PACS number(s): 73.21.−b, 73.20.Mf, 78.30.−j

Two-dimensional electron systems (2DES) exhibit a variety of physical phenomena unknown to 3D space due to the enhanced Coulomb interaction. In a perpendicular magnetic field, many-body interactions become particularly relevant, as the electron kinetic energy is completely quenched. The strong Coulomb interaction drives the 2DES into new phases of matter that have been widely discussed during recent years: incompressible fractional quantum Hall (FQH) liquids and the Wigner solid.[1] When creating systems with two spatially separated layers (bilayer system) an additional degree of freedom (pseudospin) is added. Interlayer electron-electron correlation effects are responsible for a set of FQH states, different ferromagnetic and antiferromagnetic phases.[2] The fingerprint of interlayer interaction in bilayer systems is the spectrum of collective charge-density excitations. They have been thoroughly studied experimentally in the absence of a magnetic field B, but have not so far been addressed in the presence of an external B field.

At zero field, collective charge-density excitations in the bilayer system have been discussed in Refs. 3–7. If the distance between the layers is large, the Coulomb interaction between electrons in the different layers can be neglected and each layer supports an ordinary 2D plasma excitation with a long-wavelength ($qa_B \rightarrow 0$) dispersion $\omega \sim q^{1/2}$, where q and a_B are the 2D (in-plane) momentum and the effective Bohr radius. When the distance between the layers becomes comparable with the plasma excitation wavelength, excitations in each layer couple through the interlayer Coulomb interaction. Instead of two the 2D plasmons with frequencies determined by the electron concentration in the individual layers, optical and acoustical plasma excitations with frequencies depending on the physical parameters of the system (the total concentration and distribution among the layers, the interlayer distance, and the tunnel coupling) emerge. The optical plasmon is an in-phase density fluctuation in the two electron layers with a long-wavelength dispersion of the form $\omega \sim q^{1/2}$, whereas the acoustical plasmon is an out-of-phase density fluctuation with $\omega \sim q$. Both optical and acoustical plasmons are not (or weakly) Landau damped in the long-wavelength limit.[3] The important question how optical and acoustical plasma excitations transform under an external magnetic field is discussed in the present paper.

Here, we employed resonant inelastic light scattering (ILS), one of the most powerful experimental techniques to unravel excitations in electron systems of reduced dimensionality. It is especially valuable to study out-of-phase electron-density excitations (similar to acoustical plasmons), producing no macroscopic dipole momentum and thus forbidden in infrared absorption. Another important feature of ILS is that it can distinguish through the polarization selection rules between collective charge- and spin-density excitations.[8] In the polarized geometry, incident and scattered photons have the same polarization vectors, therefore only charge-density excitations can be observed. In the depolarized geometry, polarization vectors of incident and scattered photons are perpendicular to one another, subsequently only spin-density excitations contribute to the spectra.

Symmetrically doped AlGaAs/GaAs double quantum well heterostructures were used. The GaAs quantum well (QW) thicknesses were between 200 and 300 Å and QWs were separated with an AlGaAs barrier of 25–600 Å thickness. The electron densities in the QWs (N) and mobilities ranged from 2×10^{11} to 4×10^{11} cm^{-2}, and 1×10^{6} to 2×10^{6} cm^2 V^{-1} s^{-1}. The symmetric-antisymmetric energy gap (Δ_{SAS}) varied approximately from 0 to 2 meV. If not stated otherwise, we will focus on the structure with vanishing Δ_{SAS} (i.e., disregard tunnel coupling between the quantum wells) with two equally occupied layers. The electron density in each layer equals $N_{1,2}=3.1\times10^{11}$ cm^{-2}, the QW and barrier thicknesses are 280 Å and 50 Å. The excellent quality is testified by the narrow luminescence lines of 0.3 meV. Measurements were performed in a cryostat with a 10-T superconducting coil at 1.5 K.

The ILS spectra were obtained using a Ti-sapphire laser tunable above the fundamental band gap. The excitation power density was about 0.1–1 W/cm^2. A two-fiber optical system developed by the authors was utilized to measure ILS spectra in a magnetic field.[9] One fiber was used for photoexcitation, and the other collected and conducted scattered light out of the cryostat. The in-plane momentum was transferred to the quasi-2DES via the light-scattering process. Its value

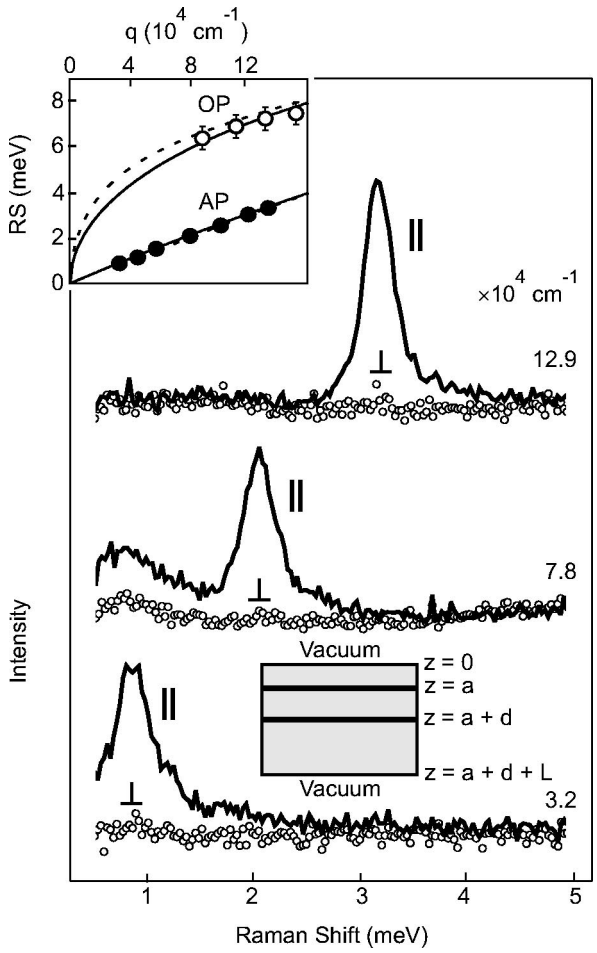

FIG. 1. ILS spectra at $B=0$ and in-plane momenta $q=3.2\times10^4, 7.8\times10^4, 12.9\times10^4$ cm^{-1} for polarized ($||$) and depolarized ($\perp$) configurations. Both QWs are equally populated, $N_{1,2}=3.1\times10^{11}$ cm^{-2}. The QW and barrier thicknesses are 280 Å and 50 Å. The inset shows the dispersion relation for acoustical and optical plasmons: experiment (dots), theory with and without the dielectric screening effect (dashed and solid lines). The bottom inset shows the sample structure.

was controlled by the arrangement of the fibers relative to the sample surface. The scattered light was dispersed in a T-64000 triple spectrograph and recorded by a charge-coupled device camera. Spectra in polarized and depolarized configurations in zero field were recorded using a cryostat with an optical window.

Making use of the ILS selection rules and the known dispersions for acoustical and optical plasmons, we identified their resonances at zero field (Figs. 1 and 2). Both optical and acoustical plasmon (AP and OP) resonances are observed only in polarized configurations of the incident and scattered photons. The AP resonance is narrower and more pronounced than the OP plasmon, a phenomenon first noted in Ref. 4. It allows for an accurate measurement of the AP dispersion in the whole range of experimentally accessible in-plane momenta, $\sim(0.2\text{–}1.4)\times10^5$ cm^{-1}. It is nearly linear and agrees well with the dispersion relation obtained from classical electrodynamics for AP excitations in two Coulomb coupled charged layers.

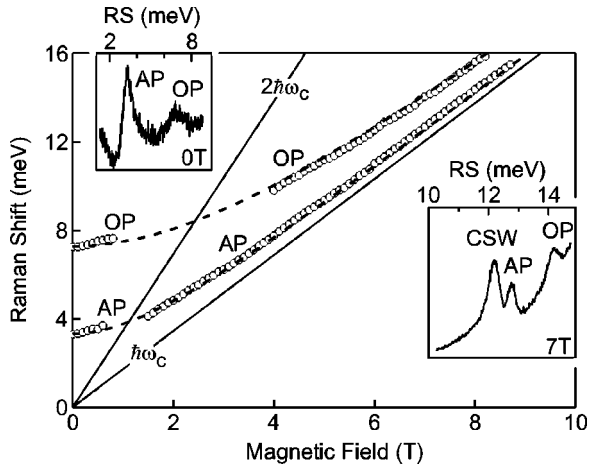

FIG. 2. The B-field dependence of the acoustical and optical plasmon energies at $q=12.9\times10^4$ cm^{-1}: experiment (dots) and theory (dashed lines). The solid lines show multiples of the cyclotron energy. Upper and lower insets: ILS spectra at $B=0$ and 7 T (Ref. 10)

We find the dispersion relations for plasma excitations using the lowest-order approximation in the spatial dispersion parameter $qa_B \ll 1$. In this case the current-field relation can be taken from the Newtonian equations of motion for electrons in the electric field of the plasma waves. The quasistatic approximation (neglecting the vortex fields) suffices, i.e., one only needs to solve the Poisson equation with appropriate boundary conditions. Let $\mathbf{u}(\mathbf{r})$ be the displacement vector of the 2D plasma; then the nonequilibrium part of the areal electron density $\tilde{N}$ is given by the relation $\tilde{N}=-N\mathrm{div}\mathbf{u}$, where N is the equilibrium concentration. From the equations of motion one easily finds for the Fourier components,

$$\tilde{N}(q)=\phi_q(z_0)\frac{eq^2N}{m^*\omega^2},$$

with ϕ_q the electrostatic potential in the plane $z=z_0$ (see the diagram in Fig. 1) and ω the frequency of the plasma oscillations. The solution of the Poisson equation takes the form $\phi_q(z<0)=Ce^{qz}$ and $\phi_q(z>a+d+L)=De^{q(a+d+L-z)}$. In the region $0<z<a+d+L$ one obtains

$$\phi_q=Ae^{-k|z-a|}+Be^{-k|z-a-d|}+Ee^{-kz}+Fe^{kz}.$$

The coefficients from A to F are found from the matching conditions at the interfaces $z=0,a,a+d,a+d+L$. The characteristic 6×6 determinant can be easily reduced to a 4×4 one. In our case L is actually a macroscopic length (of the order of 1 mm); for $qL\gg1$ the problem can be simplified further resulting in the quadratic equation,

$$\lambda_1\lambda_2+x(\lambda_1e^{-2q(a+d)}+\lambda_2e^{-2qa}-2e^{-2q(a+d)})-e^{-2qd}=0. \quad (1)$$

Here, we denote

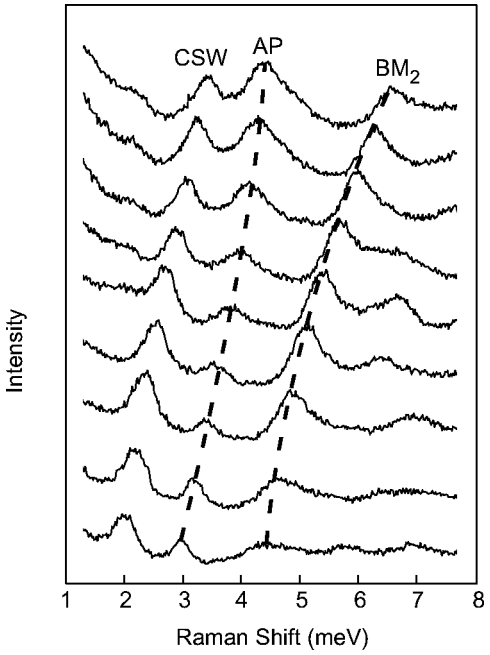

FIG. 3. The ILS spectra at the anticrossing between the acoustic plasmon and Bernstein mode with $n=2$. The spectra are shown for $B=1$ T (bottom) to 1.8 T (top) in 0.1-T steps. The dashed lines are guides to the eye.

$$\lambda_{1,2}=1-\epsilon_\infty\frac{\omega^2}{\bar{\omega}^2_{1,2}}, \tag{2}$$

$$x=\frac{\epsilon_\infty-1}{\epsilon_\infty+1}, \tag{3}$$

$$\bar{\omega}^2_{1,2}=\frac{2\pi e^2 q N_{1,2}}{m^*}, \tag{4}$$

where $\epsilon_\infty\approx 12.86$ is the background dielectric constant in GaAs, e and m^* are the electron charge and effective mass, respectively. Having incorporated the dielectric screening from the image charges at the semiconductor-vacuum boundary, the above formula generalizes the theory by Vitlina and Chaplik.[3] In the limit $a\to\infty$, Eq. (1) reduces to the familiar result:

$$\omega^2(q)=\frac{2\pi e^2 q}{\epsilon_\infty m^*}(N_1+N_2)\times\left[\frac{1}{2}\mp\frac{1}{2}\sqrt{1-\frac{4N_1N_2}{(N_1+N_2)^2}(1-e^{-2qd})}\right], \tag{5}$$

where the $-$ $(+)$ sign refers to acoustical (optical) plasmons, and d is an effective distance between the layers, a variable parameter including the nonlocality of the electron wave functions in the double QW structure. Note that even though the limit $a\to\infty$ is never achieved in a real bilayer system, the corrections to the plasmon energies due to the dielectric screening are relatively small at the studied in-plane momenta (Fig. 1). They become significant at $qa\lesssim 1$ (in our structures $a\sim 1000$ Å), so one has to take this effect into account when analyzing long-wavelength spectra, for example, far-infrared absorption spectra.

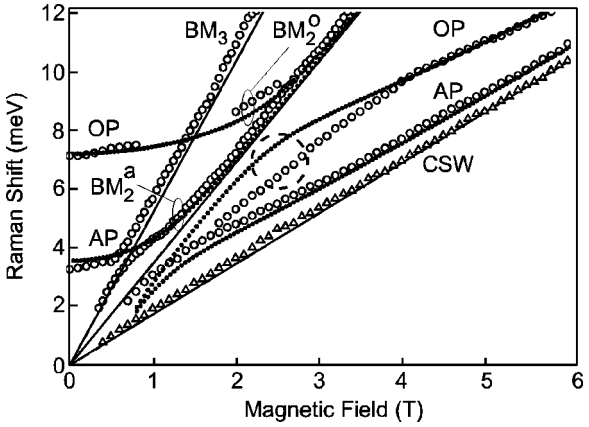

FIG. 4. Fan chart of the charge-density mode energies: experiment (large open circles) and RPA theory (small solid circles). The energy of the cyclotron spin wave (CSW) is shown as open triangles. The solid lines depict multiples of the cyclotron energy.

Having identified the ILS resonances for acoustical and optical plasmons at zero field, we studied their energies as a function of a perpendicular B field in Fig. 2–4. The entire B-field range covered is cut into two parts and these are discussed separately: the regime where the APs and OPs resonate with Bernstein modes (collective charge-density magnetoexcitations having energies $n\omega_c, n\geqslant 2$ at $ql_B\to 0$, where $\omega_c=eB/m^*c$ and $l_B=\sqrt{\hbar c/eB}$ are the cyclotron frequency and the magnetic length) and the regime where the influence of Bernstein modes (BM) on both principal plasmons can be neglected. In the latter, the energies of the principal plasmons are monotonically increasing functions of B field, slowly converging to the cyclotron energy (Fig. 2). They can be obtained in our theory by introducing the Lorenz force in the Newtonian equations of motion. The Fourier components for the nonequilibrium part $\tilde{N}$ becomes

$$\tilde{N}(q)=\phi_q(z_0)\frac{eq^2N}{(\omega^2-\omega_c^2)m^*}.$$

Equation (1) remains the same with

$$\lambda_{1,2}=1-\epsilon_\infty\frac{(\omega^2-\omega_c^2)}{\bar{\omega}^2_{1,2}}.$$

Thus, for both principal excitations one finds $\omega_B^2=\omega_0^2+\omega_c^2$, which properly covers the $B\to 0$ limit. Here, ω_B and ω_0 are the frequencies of acoustical and optical plasmons at field B and at $B=0$, respectively. As at zero field, the lower-(upper-) lying magnetoplasma mode is an out-of-phase (in-phase) charge-density fluctuation. Using the effective interlayer distance extracted from the $B=0$ data, we obtain the B-field dependencies for the optical and acoustical plasmon energies in Fig. 2.

Our model correctly describes the energies of the princi-

pal magnetoplasma excitations. Unexplained, however, is the complex anticrossing behavior close to the resonance between principal optical and acoustical magnetoplasmons and Bernstein modes (Figs. 3 and 4). This effect well known for 3D and 2D systems is often referred to as the incompressibility or nonlocality of the interacting electron system, and is governed by the electron Fermi velocity and the in-plane momentum of excitations.[11] Here, we account for these effects within a random-phase approximation (RPA). For two-component magnetoplasma in the bilayer system without tunnel coupling, the collective modes are given by the zeros of the generalized dielectric tensor ϵ_{ij} with the layer indices $i,j=1,2, \epsilon_{ij}(q,\omega)=\delta_{ij}-V_{ij}(q)\Pi_{jj}(q,\omega)$. $V_{ij}(q)$ are the intralayer and interlayer Coulomb matrix elements calculated using envelope wave functions obtained from self-consistent solutions of the Poisson and Schrödinger equations. The explicit expression for the irreducible polarizability $\Pi_{jj}(q,\omega)$ in a magnetic field (the bare bubble diagram) is given in Ref. 12. In the long-wavelength approximation, $\sim(ql_H)$,[4] which implies neglecting transitions with $\Delta n>2$, one obtains the theoretical curves in Fig. 4. The theory describes fairly well the anticrossing between the acoustical magnetoplasmon and a Bernstein mode with $n=2$ (BM_2). The decription of the anticrossing for the optical magnetoplasmon is less satisfactory. This is surprising since for single-layer systems the anticrossings between magnetoplasmon and Bernstein modes are reproduced by RPA simulations.[11] The strong energy downshift of one of the coupled modes observed here is still not understood (Fig. 4). We verified that a similar downshift occurs for bilayer systems with increased or decreased tunnel coupling. We conclude that it is related to the intralayer and interlayer Coulomb interaction, but not to the tunnel coupling.

An interesting result follows from the anticrossing picture: *there exist two Bernstein modes of different symmetry for every n*. In Fig. 4, a Bernstein mode with $n=2$ couples with the AP (BM_2^a), but does not couple with the OP. Instead, another Bernstein mode also with $n=2$ couples with the OP (BM_2^o), but in turn does not couple with the AP. Thus, experimentally the Bernstein modes can be classified as in-phase and out-of-phase modes by their interaction with the OPs or APs, respectively. Far from the anticrossing the two Bernstein modes are degenerate.

We acknowledge financial support from the Max-Planck and Humboldt Research Award, Russian Fund of Fundamental Research, the German Ministry of Science and Education (BMBF) and the German Science Foundation (DFG).

[1] For a review, see, *Perspectives in Quantum Hall Effect*, edited by S. Das Sarma and A. Pinczuk (Wiley, New York, 1997).

[2] K. Moon, H. Mori, K. Yang, S.M. Girvin, A.H. MacDonald, L. Zheng, D. Yoshioka, and S.-C. Zhang, Phys. Rev. B **51**, 5138 (1995); K. Yang, K. Moon, L. Belkhir, H. Mori, S.M. Girvin, A.H. MacDonald, L. Zheng, and D. Yoshioka, *ibid.* **54**, 11 644 (1996); L. Brey, H.A. Fertig, R. Côté, and A.H. MacDonald, *ibid.* **54**, 16 888 (1996); R.J. Radtke, S. Das Sarma, and A.H. MacDonald, *ibid.* **57**, 2342 (1998); A.H. MacDonald, R. Rajaraman, and T. Jungwirth, *ibid.* **60**, 8817 (1999).

[3] R.Z. Vitlina and A.V. Chaplik, Zh. Éksp. Teor. Fiz. **81**, 1011 (1981) [Sov. Phys. JETP **54**, 536 (1981)].

[4] D.S. Kainth, D. Richards, A.S. Bhatti, H.P. Hughes, M.Y. Simmons, E.H. Linfield, and D.A. Ritchie, Phys. Rev. B **59**, 2095 (1999).

[5] G. Gumbs and G.R. Aĭzin, Phys. Rev. B **51**, 7074 (1995).

[6] S. Das Sarma and E.H. Hwang, Phys. Rev. Lett. **81**, 4216 (1998).

[7] P.G. Bolcatto and C.R. Proetto, Phys. Rev. Lett. **85**, 1734 (2000).

[8] G. Abstreiter, M. Cardona, and A. Pinczuk, in *Light Scattering in Solid IV*, edited by M. Cardona and G. Guntherodt (Springer-Verlag, Berlin, 1984), p. 5.

[9] V.E. Kirpichev, L.V. Kulik, I.V. Kukushkin, K. von Klitzing, K. Eberl, and W. Wegscheider, Phys. Rev. B **59**, R12 751 (1999).

[10] We also observed a spin-density excitation: the cyclotron spin wave, which was identified with the symmetry test from Ref. 13.

[11] E. Batke, D. Heitmann, J.P. Kotthaus, and K. Ploog, Phys. Rev. Lett. **54**, 2367 (1985).

[12] L. Wendler and R. Pechstedt, J. Phys.: Condens. Matter **2**, 8881 (1990).

[13] L.V. Kulik, I.V. Kukushkin, V.E. Kirpichev, J.H. Smet, K. von Klitzing, and W. Wegscheider, Phys. Rev. B **63**, 201402(R) (2001); L.V. Kulik, I.V. Kukushkin, V.E. Kirpichev, J.H. Smet, K. von Klitzing, V. Umansky, and W. Wegscheider, Pis'ma Zh. Éksp. Teor. Fiz. **74**, 300 (2001) [JETP Lett. **74**, 270 (2001)].